Article

Photocatalytic Overall Water Splitting by SrTiO₃ with Surface Oxygen Vacancies

Yanfei Fan, Yan Liu, Hongyu Cui, Wen Wang, Qiaoyan Shang, Xifeng Shi, Guanwei Cui * and Bo Tang

College of Chemistry, Chemical Engineering and Materials Science, Collaborative Innovation Center of Functionalized Probes for Chemical Imaging in Universities of Shandong, Key Laboratory of Molecular and Nano Probes, Ministry of Education, Shandong Normal University, Jinan 250014, China; yffan810@163.com (Y.F.); ly2017020911@163.com (Y.L.); liuliucuicui123@163.com (H.C.); ww19862550729@163.com (W.W.); qiaoyanshang@sdnu.edu.cn (Q.S.); sxf0716@163.com (X.S.); tangb@sdnu.edu.cn (B.T.)

* Correspondence: cuiguanwei@sdnu.edu.cn

check for updates

Abstract: Strontium Titanate has a typical perovskite structure with advantages of low cost and photochemical stability. However, the wide bandgap and rapid recombination of electrons and holes limited its application in photocatalysis. In this work, a SrTiO₃ material with surface oxygen vacancies was synthesized via carbon reduction under a high temperature. It was successfully applied for photocatalytic overall water splitting to produce clean hydrogen energy under visible light irradiation without any sacrificial reagent for the first time. The photocatalytic overall water splitting ability of the as-prepared SrTiO₃-C950 is attributed to the surface oxygen vacancies that can make suitable energy levels for visible light response, improving the separation and transfer efficiency of photogenerated carriers.

Keywords: photocatalysis; water splitting; strontium titanate; oxygen vacancy; hydrogen energy

1. Introduction

Photocatalytic water splitting is a promising way to produce hydrogen clean energy [1,2]. Semiconductor materials have been widely used in this field because of their excellent photoelectric response characteristics. However, limited by the inappropriate redox potential, rapid recombination of photogenerated carriers or the backward reaction of H_2 and O_2 to H_2O, most of them can only perform the semi-reaction of water splitting to produce hydrogen or oxygen alone assisted by sacrificial agents such as methanol, sodium sulfite or silver nitrate [3,4]. Therefore, although photocatalytic water splitting has been studied for several decades, there are few reported materials that can realize overall water splitting, which still remains a challenge in the photocatalytic research field [5–8].

Strontium Titanate (SrTiO₃) has typical perovskite structure with the advantages of low cost and excellent chemical stability. It has been widely used as a photocatalyst [9,10]. However, due to the wide band gap, it can only utilize ultraviolet light (about 5% of sunlight) during photocatalytic reactions. Moreover, although its band structure suits the water redox potential levels [11], SrTiO₃ powders alone cannot decompose water into H_2 and O_2 simultaneously because of rapid recombination of photogenerated carriers or fast backward reaction. It is necessary to modify the SrTiO₃ particle to obtain an active photocatalyst for water splitting. Up to now, many outstanding methods, such as doped with metals or non-metals [12–16], or coupled with other semiconductors [17], have been investigated to solve the abovementioned issues. Recently, a modified aluminum-doped strontium titanate (SrTiO₃: Al) photocatalyst was applied to perform overall water splitting with an external quantum efficiency of up to 96 per cent, which was still performed under UV light irradiation [18].

Oxygen vacancies on a particle surface often act as active sites and play an important role in photocatalytic reactions [19]. Moreover, they can provide trapping sites for photogenerated carriers and prevent them from rapid recombination. Most notably, they can build a surface energy state that can narrow the band gap, expanding the solar absorbance range to lower energy wavelengths [20]. Thus, rational control of oxygen vacancies on the catalyst surface is extremely important for improving the photocatalytic efficiency [21–23]. Although there are usually many oxygen vacancies in the inner part of bulk $SrTiO_3$, they do not contribute to the sub-band gap photoexcitation or intrinsic magnetism of $SrTiO_3$, and are different from the surface oxygen vacancies [20]. Therefore, it is necessary to synthesize $SrTiO_3$ materials with abundant surface oxygen vacancies to realize overall photocatalytic water splitting under visible light conditions. Carbon material is a cheap and safe reductant that can capture oxygen atoms from the oxide surface to produce reductive species or create oxygen vacancies at a high temperature [24,25]. Herein, it was found that when the pristine $SrTiO_3$ was heated under reducing atmosphere afforded by carbon, a disordered surface layer with amounts of oxygen vacancies was obtained. The as-prepared $SrTiO_3$ with a grey color showed overall photocatalytic water splitting ability under visible light irradiation without a sacrifice reagent.

2. Materials and Methods

2.1. Materials

Ti(C$_4$H$_9$O)$_4$,Sr(NO$_3$)$_2$, KOH, ammonia, NaClO$_4$, terpinol, naphthol, polyvinyl alcohol (PVA), ethanol and active carbon power were purchased from Sinopharm Chemical Reagent Company. All the chemicals were of AR grade. Ultrapure water used in the experiment was Wahaha pure water.

2.2. Synthesis of SrTiO$_3$-C950

$SrTiO_3$ was synthesized by a hydrothermal method [26]. Typically, Ti(C$_4$H$_9$O)$_4$ (2.72 g) and ethanol (70.00 mL) were mixed homogeneously by stirring at room temperature. Then, ammonia solution (2.50 mL of ammonia diluted with 30.00 mL of ethanol) was added to the mixed solution with stirring for one hour. The obtained precipitate was washed with distilled water several times and dispersed in 80.00 mL distilled water with vigorous stirring. Then, 5.08 g Sr(NO$_3$)$_2$, 2.24 g KOH, and 0.32 g polyvinyl alcohol (PVA) were added to the mixture solution. Finally, the obtained suspension was transferred into a stainless-steel Teflon-lined autoclave and heated at 180 °C for 12 h. The obtained solid product was washed with diluted nitric acid, distilled water and ethanol several times in turn and then dried at 80 °C for 4 h. Finally, the as-prepared $SrTiO_3$ (0.50 g) and carbon (0.08 g) were well mixed. The mixture was calcined at 950 °C for 3 h with a heating rate of 5 °C/min under N$_2$ atmosphere, and then naturally cooled at room temperature. The as-prepared sample was denoted as $SrTiO_3$-C950. The mixture of $SrTiO_3$ (0.50 g) and carbon (0.08 g) calcined at 300 °C for 3 h with a heating rate of 5 °C/min under N$_2$ atmosphere, denoted as $SrTiO_3$-C300, was used as reference samples.

2.3. Electrochemical Measurements

The photocurrent was measured by an electrochemical analyzer (CHI660D Instruments, Shanghai Chenhua Instrument Co., Ltd., Shanghai, China) with a standard three-electrode system. The electrolyte was a 0.10 M NaClO$_4$ aqueous solution. The working electrode was prepared as follows. The slurry was obtained by grinding a mixture of the sample (0.05 g) and terpinol (0.10 g). Then, the slurry was coated onto a 4.00 cm × 1.00 cm indium tin oxide-coated glass (ITO glass) electrode by the doctor blade technique, dried in an oven, and calcined at 290 °C for 30 min under Ar conditions. The as-prepared sample, Pt sheet and saturated calomel electrode were used as the working electrode, counter electrode and reference electrode, respectively. Prior to the photocurrent measurements, the electrolyte (0.10 M NaClO$_4$, pH = 6.56) was purged with Ar for 30 min.

The electrochemical impedance test was also carried out with a standard three-electrode system. The glassy carbon electrode deposited with the as-prepared samples was used as the working electrode.

Pt sheet and saturated calomel electrode was used as the counter electrode and the reference electrode, respectively. The working electrode was prepared as follows: 4.00 mg the as-prepared sample was dispersed in 1.00 mL mixture of water and isopropanol with the volume ratio of 3:1, then 40.00 μL naphthol was added into the mixture and ultrasonicated for 30 min. The obtained slurry was dropped onto the glassy carbon electrode, and then dried naturally at room temperature. Finally, the prepared working electrode, counter electrode and reference electrode were immersed in a deionized water solution for testing.

2.4. Photocatalytic Water Splitting

The photocatalytic water splitting reaction was performed using an XPA-7 photocatalytic reaction instrument (Xujiang Electromechanical Plant, Nanjing, China). In a typical process, 0.40 g $SrTiO_3$-C950, 0.20 g La_2O_3 and 10.00 mL water were mixed in a 20 mL quartz bottle at room temperature. The bottle was sealed with a silicone rubber septum. The suspension was thoroughly deaerated and purged with N_2 for 30 min before the photocatalysis experiment. Then, the suspension was irradiated by a 1000 W Xe lamp with or without light cutoff filters ($\lambda > 420$ nm) under ambient conditions and magnetic stirring for a certain time. The gaseous production was analyzed by gas chromatography (FULI 9750, TCD, argon as the carrier gas, and 5 Å molecular sieve column).

The solar-to-hydrogen (STH) conversion efficiency was evaluated by using a 1000 W Xe lamp as the light source and 0.40 g catalyst in water. After irradiation for 48 h, an average of 360 μmol H_2 was obtained, which corresponds to 93 J free energy. The incident light power was 162 mW/cm^2, which was measured by a handheld Optical Power Meter (Newport 1916-R). The Light exposure area of the quartz bottle is about 3.84 cm^2. Therefore, the total incident energy over the quartz bottle was about 107,495 J in 48 h. A solar-to-hydrogen efficiency of 0.09% was obtained, assuming all incident light was absorbed by optically thick nanoparticle suspension, which was obtained by the following calculation formula: Solar-to-hydrogen efficiency = Output energy of hydrogen generated/Energy of incident light = 93/107495 = 0.09% [1,27].

3. Results and Discussion

Irregular spherical $SrTiO_3$ particles with diameters of 100–300 nm were synthesized by a hydrothermal method (Figure 1a) [26]. The carbon reduction process was performed under different calcination temperatures and retention time. It was found that the samples obtained under calcination temperature of 950 °C and a retention time of 3 h under N_2 atmosphere (marked as $SrTiO_3$-C950) and showed the highest photocatalytic activity. Compared with uncalcined $SrTiO_3$ particles, the as-prepared $SrTiO_3$-C950 particles showed larger particle size (Figure 1b) because of the Ostwald ripening under a high temperature, which was further determined by a laser particle size analyzer (Figure S1). The as-prepared $SrTiO_3$ calcined at 950 °C for 3 h with a heating rate of 5 °C/min under air atmosphere was used as a reference sample. As shown in Figure 1c, the X-ray diffraction (XRD) peaks at 22.78, 32.42, 39.98, 46.48, 52.35, 57.79, 67.80, 72.54 and 77.18 can be attributed to the Miller indices of (100), (110), (111), (200), (210), (211), (220), (300) and (310), which can be indexed to the standard cubic perovskite structure (space group: Pm3m) of $SrTiO_3$ (JPCDS No. 35–734) without any crystalline by-product. There is no obvious difference in XRD patterns of $SrTiO_3$-C950 and the reference $SrTiO_3$. This result indicates that the overall crystal structure of $SrTiO_3$ is not fundamentally changed under high temperature reduction treatment. No obvious diffraction peaks of graphite carbon are observed due to its amorphous phase or low residue.

As shown in Figure 2b, a highly disordered layer with a thickness of 2.0 nm was formed on the surface of $SrTiO_3$ after carbonization. It is ascribed to the presence of a large number of oxygen vacancies on the surface of $SrTiO_3$ particles caused by the reduction treatment under a high temperature [28], which is further confirmed by EPR and X-ray photoelectron spectroscopy (XPS) analysis. The produced surface oxygen vacancies will act as an electron-trapping center, showing EPR signals. Therefore, EPR is one of the most powerful methods to identify the presence of oxygen vacancies in the solid

materials [29]. The low-field signal with g-factor (g is the spectroscopic splitting factor in the case of a free electron) close to the free-electron value (g = 2.0023) is generally attributed to an unpaired electron trapped on an oxygen vacancy site. If the g-value of the light-induced EPR signal is smaller than that of a free electron, 2.0023, the signal is due to the trapped electron. Herein, as shown in Figure 2c, the EPR signal of $SrTiO_3$-C950 with a g-value of 1.97 is due to the electrons captured by the oxygen vacancies. As a comparison, there are no EPR signals at the same position observed for $SrTiO_3$.
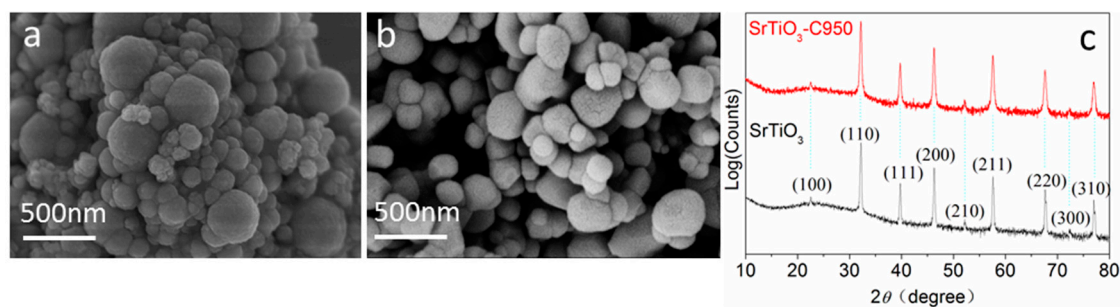
Figure 1. Morphology and Structure characterizations of $SrTiO_3$. (**a**), Scanning Electron Microscope (SEM) image of $SrTiO_3$; (**b**), SEM of $SrTiO_3$-C950; (**c**), XRD of $SrTiO_3$ and $SrTiO_3$-C950.
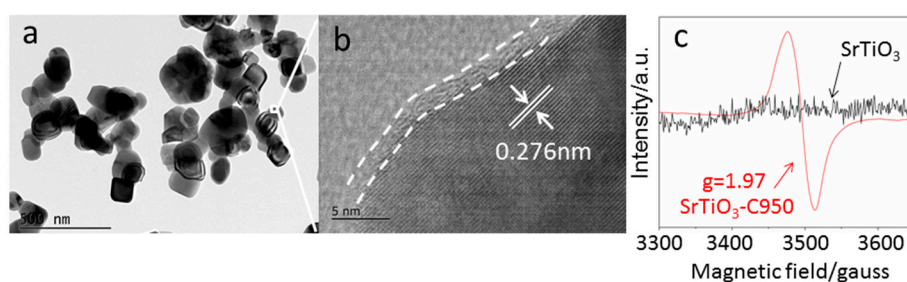

Figure 2. Transmission Electron Microscope (TEM) image (**a**), High Resolution Transmission Electron Microscope (HRTEM) image (**b**) and Electron Paramagnetic Resonance (EPR) image (**c**) of $SrTiO_3$-C950.

The chemical states of Sr, Ti, O and C in $SrTiO_3$ and $SrTiO_3$-C950 were determined by XPS spectra (Figure S2). As shown in Figure 3a–d, compared with $SrTiO_3$, $SrTiO_3$-C950 shows distinctly different XPS peaks. The Sr^{2+} 3d5/2 peak centered at 135.58 eV, 136.88 eV and the O1s peak centered at 530.87 eV ascribed to the SrO crystal phase and are observed on $SrTiO_3$-C950 (Figure 3a,b) [30]. The as-prepared $SrTiO_3$-C950 samples showed the same two Ti2p peaks centered at 458.04 eV (Peak 1) and 463.64 eV (Peak 2) with the referenced $SrTiO_3$. However, three reduced titanium ion XPS peaks centered at 457.18 eV (Peak 3), 460.3 eV (Peak 4) and 465.48 eV (Peak 5) were observed for $SrTiO_3$-C950, which could be ascribed to the low valence state titanium of nonstoichiometric TiO_{2-x} (0 < X < 2) species, mainly including Ti^{2+} 2p1/2 of TiO (Figure 3c) [31,32], which are quite different from the titanium ion XPS peaks of the $SrTiO_3$. The new appearance of SrO and reduced Ti species indicates that there is a large number of oxygen vacancies existing in the surface layer of $SrTiO_3$-C950 [33]. Meanwhile, it preliminary indicates that the surface of $SrTiO_3$-C950 may be mainly composed of SrO and TiO species layers [34]. The SrO surface layers of $SrTiO_3$ was thought to have higher water adsorption dissociation ability [35], which may be more helpful for the photocatalytic water splitting. Because of the existence of carbon standard materials for the XPS test, both the pristine $SrTiO_3$ and $SrTiO_3$-C950 show obvious carbon peaks (Figure 3d). However, there are significant differences between them on the XPS C1s peaks. For the $SrTiO_3$-C950, a C1s peak centered at 285.67 eV ascribed to β-carbon connected with the oxygenic groups on the alkyl chain is believed to originate from carbon reductant [36]. It indicates that there is still a small amount of residual carbon on the surface of strontium titanate. There are no C1s peaks attributed to TiC observed for $SrTiO_3$-C950 and pristine $SrTiO_3$ [37], indicating that carbon atoms are not doped into a strontium titanate lattice during the reduction process.
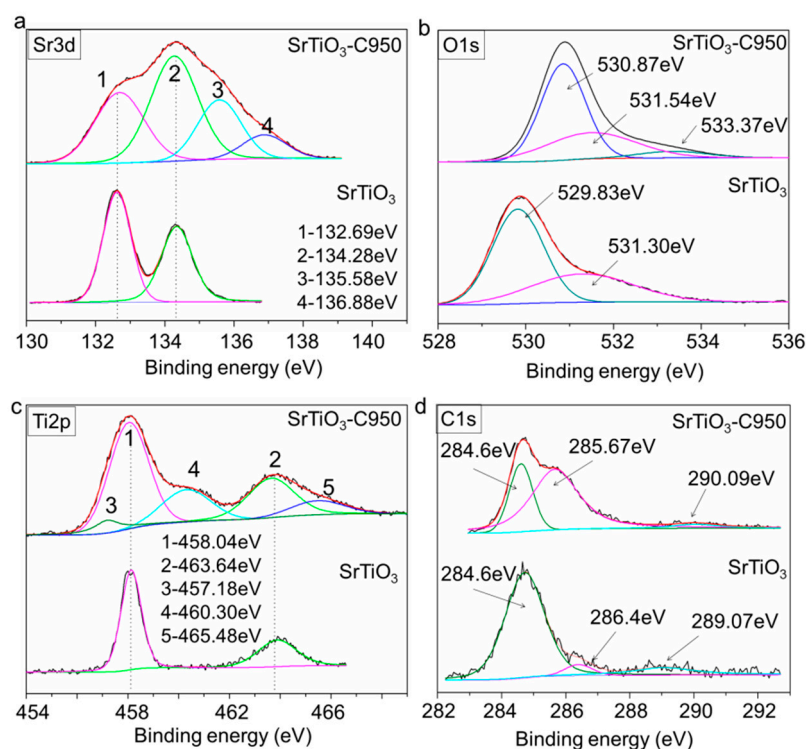
Figure 3. XPS spectra of Sr3d (**a**), O1s (**b**), Ti2p (**c**) and C1s (**d**) of $SrTiO_3$ and $SrTiO_3$-C950.

The photocatalytic activity of $SrTiO_3$-C950 and pristine $SrTiO_3$ was evaluated by photocatalytic water splitting under Xe lamp light irradiation with or without light cutoff filters ($\lambda > 420$ nm) (Figure 4). Compared with pristine $SrTiO_3$, the as-prepared $SrTiO_3$-C950 shows an obvious photocatalytic water splitting capability with a solar-to-hydrogen (STH) conversion efficiency of 0.09% without any sacrificial reagent. Under the optimal photocatalytic reaction conditions, the average H_2 evolution rate and O_2 evolution rate of $SrTiO_3$-C950 is 20.6 umol/g×h and 7.5 umol/g·h under Xe lamp light irradiation, respectively (Figure 4a). Under the visible light irradiation, the average H_2 evolution rate and O_2 evolution rate of $SrTiO_3$-C950 are 2.3 μmol/g×h and 1.0 μmol/g·h, respectively (Figure 4b). There is no noticeable difference in the photocatalytic activity of $SrTiO_3$-C950 under different pH conditions. In this work, the evolution rates ratio of O_2 and H_2 are 0.7:2, which is lower than that of the theoretical stoichiometrically ratio 1:2 of water splitting. This phenomenon has been observed in many water splitting systems, which is due to the produced O_2 or intermediate oxygen species being readily absorbed by the metal elements to form steady peroxide complexes [38,39].

Although pristine $SrTiO_3$ has suitable energy band structure for the water redox potential levels [11], it cannot decompose water into H_2 and O_2 simultaneously because of rapid recombination of photogenerated carriers or fast backward reaction. According to the previous reports, it is proposed that the residual carbon on the surface of $SrTiO_3$-C950 is favorable for improving the photocatalytic efficiency [40]. However, a referenced $SrTiO_3$ modified with carbon calcinated under 300 °C temperatures without reduction treatment, showed no photoactivity on overall water splitting. Therefore, herein, the photocatalytic overall water splitting ability of the as-prepared $SrTiO_3$-C950 was suggested to be owed to the surface oxygen vacancies that can make suitable energy levels for visible light response and improve the separation and transfer efficiency of photogenerated carriers [41].

As shown in Figure 5a, compared with $SrTiO_3$, the absorption wavelength of $SrTiO_3$-C950 shows an obvious red shift to the visible light region. Estimated from the UV-V is the DRS absorption tail, the band gap of $SrTiO_3$-C950 is 2.92 eV, which is significantly smaller than that of $SrTiO_3$ with 3.10 eV. It is due to the formation of the mid-gap states between the valence band and the conduction band, which is attributed to surface oxygen vacancies [19]. These mid-gap states can form a continuum

extending to and overlapping with the conduction band edges in a result of narrowing the band gap and expanding the solar absorbance range to lower energy waves. As shown in Figure 5b, obtained from the XPS valence band spectrum (VBXPS), the valence band edge of pristine $SrTiO_3$ is localized at 1.94 eV below the Fermi level. Then, it is calculated that the conduction band minimum would localize at about -1.16 eV. The valence band edge of $SrTiO_3$-C950 expands to 1.82 eV. In the same way, combined with the band gap of 2.92 eV from optical measurements, the conduction band minimum edge of $SrTiO_3$-C950 expands to -1.10 eV. Therefore, the formed energy band structure of $SrTiO_3$-C950 is suitable for photocatalytic water splitting under visible light irradiation.
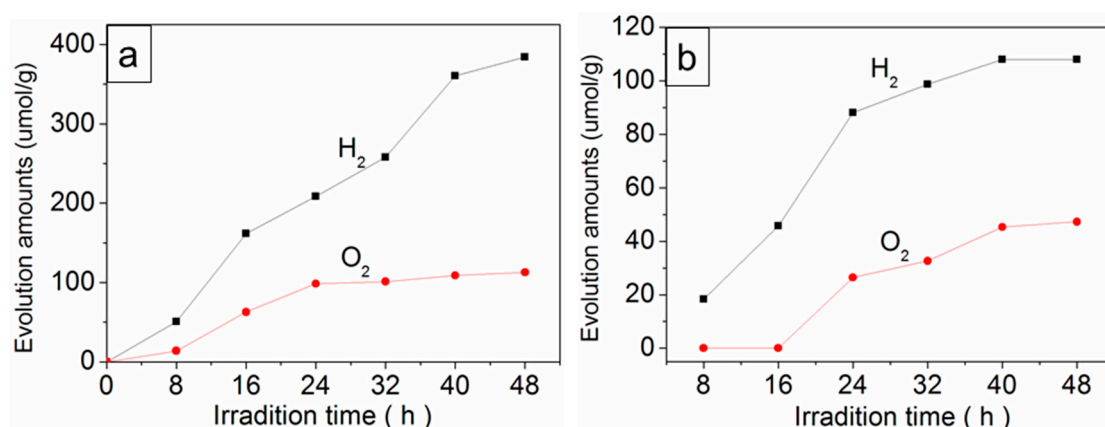

Figure 4. Photocatalytic activity of $SrTiO_3$-C950 under full-spectrum light irradiation (**a**) or visible light irradiation (**b**) without sacrificial reagent. No photocatalytic water splitting activity was observed for pristine $SrTiO_3$ and $SrTiO_3$-C300 under the same conditions.
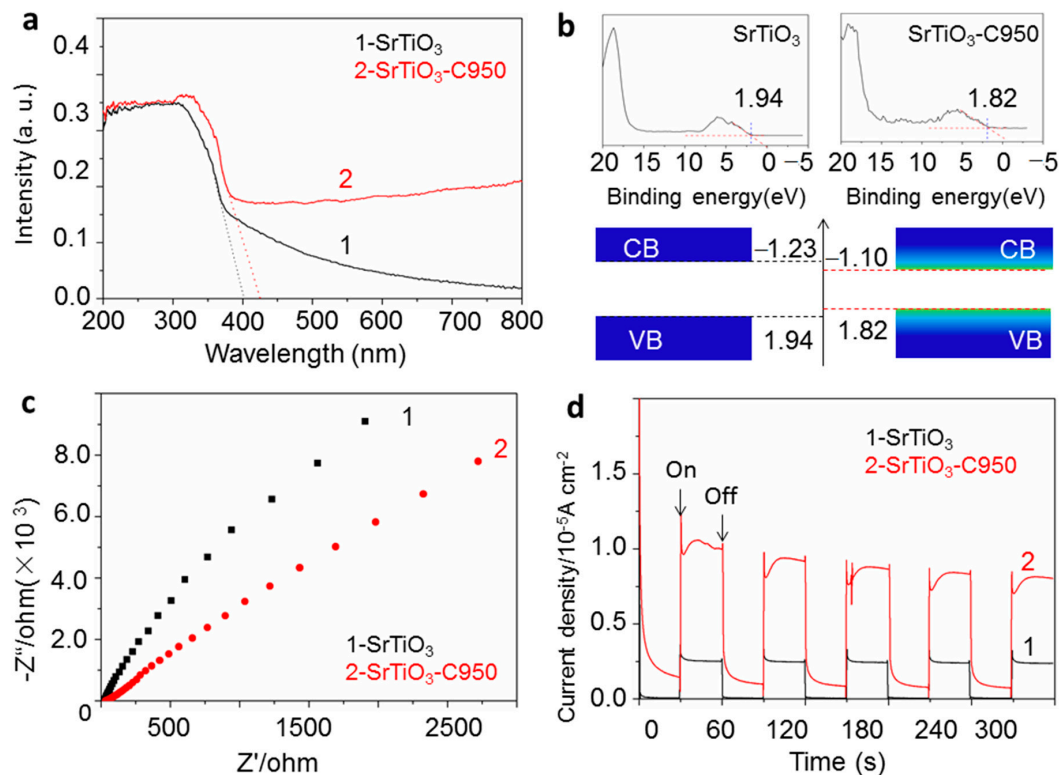

Figure 5. Ultraviolet–visible diffuse reflectance spectrum (UV-Vis DRS) (**a**), XPS Valence Band Spectrum and Energy band structure of $SrTiO_3$ (left) and $SrTiO_3$-C950 (right) (**b**), Electrochemical impedance spectroscopy (**c**) and Photocurrent density (**d**) of $SrTiO_3$-C950 and $SrTiO_3$.

In addition, because of the presence of free electrons bounded loosely in the oxygen vacancies [42–44], the surface electric conductivity of $SrTiO_3$-C950 will be improved, as a result of improving the carriers' transfer efficiency, which is also helpful for improving the photocatalytic activity. The electrochemical impedance spectroscopy (Nyquist plot) was used to determine the charge transfer ability. The pristine $SrTiO_3$ and $SrTiO_3$-C950 all show a classical semicircular Nyquist diagram (Figure 5c). The arc radius of $SrTiO_3$-C950 is obviously smaller than that of $SrTiO_3$, which indicates that the photogenerated charges in $SrTiO_3$-C950 would suffer less resistance than that of $SrTiO_3$ and obtain a higher transfer rate. The photocurrent density of $SrTiO_3$-C950 was much higher than that of pristine $SrTiO_3$ under Xe lamp light irradiation (Figure 5d), which indicates that the charge separation in $SrTiO_3$-C950 has been enhanced remarkably. Herein, the photocurrent density of $SrTiO_3$-C950 shows a slow decrease with the following cycles, which may be due to the destruction of surface oxygen vacancies under the presence of external electric fields during a photocurrent test. It is proposed that, besides the aforementioned two factors, the higher charge separation efficiency is ascribed to the temporary storage capacity of surface oxygen vacancies for photogenerated carriers [21,45]. Moreover, according to the previous reports, the formed surface oxygen vacancies and SrO species are proposed to be more favorable for the adsorption and decomposition of water molecules [30].

4. Conclusions

In summary, a $SrTiO_3$ material with surface oxygen vacancies was synthesized by carbon reduction under a high temperature. The as-prepared $SrTiO_3$-C950 was successfully applied in photocatalytic water splitting research under visible light irradiation without any sacrificial reagent for the first time. The photocatalytic overall water splitting ability of the as-prepared $SrTiO_3$-C950 is attributed to the surface oxygen vacancies that can make suitable energy levels for a visible light response, improve the separation and transfer efficiency of photogenerated carriers. In addition, according to the previous reports, it is proposed that the formed surface oxygen and SrO species is proposed to be more favorable for the adsorption and decomposition of water molecular. This work provided a strategy to design efficient photocatalysts by constructing oxygen vacancies.

Author Contributions: Conceptualization, G.C.; methodology, Y.L. and W.W.; validation, Y.F. and X.S.; investigation, Y.L.; writing—original draft preparation, H.C. and Q.S.; writing—review and editing, G.C.; supervision, B.T.; project administration, B.T.; funding acquisition, B.T. All authors have read and agreed to the published version of the manuscript.

Conflicts of Interest: The authors declare no conflict of interest. The funders had no role in the design of the study; in the collection, analyses, or interpretation of data; in the writing of the manuscript, or in the decision to publish the results.

References

1. Zhao, Q.; Zhang, Q.; Du, C.; Sun, S.; Steinkruger, J.D.; Zhou, C.; Yang, S. Synergistic effect of dual particle size AuNPs on TiO_2 for efficient photocatalytic hydrogen evolution. *Nanomaterials* **2019**, *9*, 499. [CrossRef]
2. Zhang, G.; Wang, X. Oxysulfide semiconductors for photocatalytic overall water splitting with visible light. *Angew. Chem. Int. Ed.* **2019**, *58*, 15580–15582. [CrossRef]
3. Tee, S.Y.; Win, K.Y.; Teo, W.S.; Koh, L.-D.; Liu, S.; Teng, C.P.; Han, M.-Y. Recent progress in energy-driven water splitting. *Adv. Sci.* **2017**, *4*, 1600337. [CrossRef]

4. Zhao, H.; Zhang, H.; Cui, G.; Dong, Y.; Wang, G.; Jiang, P.; Wu, X.; Zhao, N. A photochemical synthesis route to typical transition metal sulfides as highly efficient cocatalyst for hydrogen evolution: From the case of NiS/g-C_3N_4. *Appl. Catal. B Environ.* **2018**, *225*, 284–290. [CrossRef]

5. Chen, S.; Takata, T.; Domen, K. Particulate photocatalysts for overall water splitting. *Nat. Rev. Mater.* **2017**, *2*, 17050. [CrossRef]

6. Ismael, M.; Wu, Y. A mini-review on the synthesis and structural modification of g-C_3N_4-based materials, and their applications in solar energy conversion and environmental remediation. *Sustain. Energy Fuels* **2019**, *3*, 2907–2925. [CrossRef]

7. Lu, D.; Ouyang, S.; Xu, H.; Li, D.; Zhang, X.; Li, Y.; Ye, J. Designing Au Surface-Modified Nanoporous-Single-Crystalline $SrTiO_3$ to Optimize Diffusion of Surface Plasmon Resonance-Induce Photoelectron toward Enhanced Visible-Light Photoactivity. *ACS Appl. Mater. Inter.* **2016**, *8*, 9506–9513. [CrossRef]

8. Cui, G.; Wang, W.; Ma, M.; Xie, J.; Shi, X.; Deng, N.; Xin, J.; Tang, B. IR-Driven Photocatalytic Water Splitting with WO_2–Na_xWO_3 Hybrid Conductor Material. *Nano Lett.* **2015**, *15*, 7199–7203. [CrossRef]

9. Iwashina, K.; Kudo, A. Rh-doped $SrTiO_3$ photocatalyst electrode showing cathodic photocurrent for water splitting under visible-light irradiation. *J. Am. Chem. Soc.* **2011**, *133*, 13272–13275. [CrossRef]

10. Sangle, A.L.; Singh, S.; Jian, J.; Bajpe, S.R.; Wang, H.; Khare, N.; MacManus-Driscoll, J.L. Very high surface area mesoporous thin films of $SrTiO_3$ grown by pulsed laser deposition and application to efficient photoelectrochemical water splitting. *Nano Lett.* **2016**, *16*, 7338–7345. [CrossRef]

11. Puangpetch, T.; Sreethawong, T.; Yoshikawa, S.; Chavadej, S. Hydrogen production from photocatalytic water splitting over mesoporous-assembled $SrTiO_3$ nanocrystal-based photocatalysts. *J. Mol. Catal. A Chem.* **2009**, *312*, 97–106. [CrossRef]

12. Yamaguchi, Y.; Terashima, C.; Sakai, H.; Fujishima, A.; Kudo, A.; Nakata, K. Photocatalytic degradation of gaseous acetaldehyde over Rh-doped $SrTiO_3$ under visible light irradiation. *Chem. Lett.* **2016**, *45*, 42–44. [CrossRef]

13. Bi, Y.; Ehsan, M.F.; Huang, Y.; Jin, J.; He, T. Synthesis of Cr-doped $SrTiO_3$ photocatalyst and its application in visible-light-driven transformation of CO_2 into CH_4. *J. CO2 Util.* **2015**, *12*, 43–48. [CrossRef]

14. Liu, P.; Nisar, J.; Pathak, B.; Ahuja, R. Hybrid density functional study on $SrTiO_3$ for visible light photocatalysts. *Int. J. Hydrogen Energy* **2012**, *37*, 11611–11617. [CrossRef]

15. Zou, F.; Jiang, Z.; Qin, X.; Zhao, Y.; Jiang, L.; Zhi, J.; Xiao, T.; Edwards, P.P. Template-free synthesis of mesoporous N-doped $SrTiO_3$ perovskite with high visible-light-driven photocatalytic activity. *Chem. Commun.* **2012**, *48*, 8514–8516. [CrossRef]

16. Chen, W.; Liu, H.; Li, X.; Liu, S.; Gao, L.; Mao, L.; Fan, Z.; Shangguan, W.; Fang, W.; Liu, Y. Polymerizable complex synthesis of $SrTiO_3$: (Cr/Ta) photocatalysts to improve photocatalytic water splitting activity under visible light. *Appl. Catal. B Environ.* **2016**, *192*, 145–151. [CrossRef]

17. Wang, Q.; Hisatomi, T.; Jia, Q.; Tokudome, H.; Zhong, M.; Wang, C.; Pan, Z.; Takata, T.; Nakabayashi, M.; Shibata, N.; et al. Scalable water splitting on particulate photocatalyst sheets with a solar-to-hydrogen energy conversion efficiency exceeding 1%. *Nat. Mater.* **2016**, *15*, 611–615. [CrossRef]

18. Takata, T.; Jiang, J.; Sakata, Y.; Nakabayashi, M.; Shibata, N.; Nandal, V.; Seki, K.; Hisatomi, T.; Domen, K. Photocatalytic water splitting with a quantum efficiency of almost unity. *Nature* **2020**, *581*, 411–414. [CrossRef] [PubMed]

19. Zhao, X.; Feng, J.; Chen, S.; Huang, Y.; Sum, T.C.; Chen, Z. New insight into the roles of oxygen vacancies in hematite for solar water splitting. *Phys. Chem. Chem. Phys.* **2017**, *19*, 1074–1082. [CrossRef]

20. Choi, H.; Song, J.D.; Lee, K.-R.; Kim, S. Correlated visible-light absorption and intrinsic magnetism of $SrTiO_3$ due to oxygen deficiency: Bulk or surface effect? *Inorg. Chem.* **2015**, *54*, 3759–3765. [CrossRef]

21. Wang, G.; Ling, Y.; Li, Y. Oxygen-deficient metal oxide nanostructures for photoelectrochemical water oxidation and other applications. *Nanoscale* **2012**, *4*, 6682–6691. [CrossRef] [PubMed]

22. Chen, X.; Liu, L.; Yu, P.Y.; Mao, S.S. Increasing solar absorption for photocatalysis with black hydrogenated titanium dioxide nanocrystals. *Science* **2011**, *331*, 746–750. [CrossRef] [PubMed]

23. Feng, H.; Xu, Z.; Ren, L.; Liu, C.; Zhuang, J.; Hu, Z.; Xu, X.; Chen, J.; Wang, J.; Hao, W.; et al. Activating titania for efficient electrocatalysis by vacancy engineering. *ACS Catal.* **2018**, *8*, 4288–4293. [CrossRef]

24. Hamdy, M.S.; Amrollahi, R.; Mul, G. Surface Ti^{3+}-containing (blue) titania: A unique photocatalyst with high activity and selectivity in visible light-stimulated selective oxidation. *ACS Catal.* **2012**, *2*, 2641–2647. [CrossRef]

25. Zuo, F.; Wang, L.; Wu, T.; Zhang, Z.; Borchardt, D.; Feng, P. Self-doped Ti^{3+} enhanced photocatalyst for hydrogen production under visible light. *J. Am. Chem. Soc.* **2010**, *132*, 11856–11857. [CrossRef] [PubMed]

26. Wei, X.; Xu, G.; Ren, Z.; Xu, C.; Weng, W.; Shen, G.; Han, G. Single-crystal-like mesoporous SrTiO$_3$ spheres with enhanced photocatalytic performance. *J. Am. Ceram. Soc.* **2010**, *93*, 1297–1305.

27. Liao, L.; Zhang, Q.; Su, Z.; Zhao, Z.; Wang, Y.; Li, Y.; Lu, X.; Wei, D.; Feng, G.; Yu, Q.; et al. Efficient solar water-splitting using a nanocrystalline CoO photocatalyst. *Nat. Nanotechnol.* **2014**, *9*, 69–73. [CrossRef]

28. Shutthanandan, V.; Thevuthasan, S.; Liang, Y.; Adams, E.M.; Yu, Z.; Droopad, R. Direct observation of atomic disordering at the SrTiO$_3$/Si interface due to oxygen diffusion. *Appl. Phys. Lett.* **2002**, *80*, 1803–1805. [CrossRef]

29. Kinoshita, T.; Yamazaki, M.; Kawazoe, H.; Hosono, H. Long lasting phosphorescence and photostimulated luminescence in Tb-ion-activated reduced calcium aluminate glasses. *J. Appl. Phys.* **1999**, *86*, 3729–3733. [CrossRef]

30. Van Doveren, H.; Verhoeven, J.A.T.H. XPS spectra of Ca, Sr, Ba and their oxides. *J. Electron Spectrosc. Relat. Phenom.* **1980**, *21*, 265–273. [CrossRef]

31. Franzen, H.F.; Umana, M.X.; McCreary, J.R.; Thorn, R.J. XPS spectra of some transition metal and alkaline earth monochalcogenides. *J. Solid State Chem.* **1976**, *18*, 363–368. [CrossRef]

32. Gonbeau, D.; Guimon, C.; Pfister-Guillouzo, G.; Levasseur, A.; Meunier, G.; Dormoy, R. XPS study on thin films of titanium oxysulfides. *Surf. Sci.* **1991**, *254*, 81–89. [CrossRef]

33. Ling, Y.; Wang, G.; Reddy, J.; Wang, C.; Zhang, J.Z.; Li, Y. The influence of oxygen content on the thermal activation of hematite nanowires. *Angew. Chem. Int. Ed.* **2012**, *51*, 4074–4079. [CrossRef] [PubMed]

34. Bachelet, R.; Sánchez, F.; Palomares, F.J.; Ocal, C.; Fontcuberta, J. Atomically flat SrO-terminated SrTiO$_3$(001) substrate. *Appl. Phys. Lett.* **2009**, *95*, 141915. [CrossRef]

35. Li, W.; Liu, S.; Wang, S.; Guo, Q.; Guo, J. The roles of reduced Ti cations and oxygen vacancies in water absorption and dissociation on SrTiO$_3$(110). *J. Phys. Chem. C* **2014**, *118*, 2469–2474. [CrossRef]

36. Mazzanti, J.B.; Reamey, R.H.; Helfand, M.A.; Lindley, P.M. Surface studies of solvent-cast poly(vinyl-co-vinyl acetate) copolymer films. *J. Vac. Sci. Technol. A* **1992**, *10*, 2419–2424. [CrossRef]

37. Galuska, A.A.; Uht, J.C.; Marquez, N. Reactive and nonreactive ion mixing of Ti films on carbon substrates. *J. Vac. Sci. Technol. A* **1988**, *6*, 110–122. [CrossRef]

38. Duonghong, D.; Grätzel, M. Colloidal TiO$_2$ particles as oxygen carriers in photochemical water cleavage systems. *J. Chem. Soc. Chem. Commun.* **1984**, *23*, 1597–1599. [CrossRef]

39. Liu, J.; Zhang, Y.; Lu, L.; Wu, G.; Chen, W. Self-regenerated solar-driven photocatalytic water-splitting by urea derived graphitic carbon nitride with platinum nanoparticles. *Chem. Commun.* **2012**, *48*, 8826–8828. [CrossRef]

40. Chen, C.; Long, M.; Zeng, H.; Cai, W.; Zhou, B.; Zhang, J.; Wu, Y.; Ding, D.; Wu, D. Preparation, characterization and visible-light activity of carbon modified TiO$_2$ with two kinds of carbonaceous species. *J. Mol. Catal. A Chem.* **2009**, *314*, 35–41. [CrossRef]

41. Reihl, B.; Bednorz, J.G.; Muller, K.A.; Jugnet, Y.; Landgren, G.; Morar, J.F. Electronic structure of strontium titanate. *Phys. Rev. B* **1984**, *30*, 803–806. [CrossRef]

42. Deskins, N.A.; Rousseau, R.; Dupuis, M. Distribution of Ti^{3+} surface sites in reduced TiO$_2$. *J. Phys. Chem. C* **2011**, *115*, 7562–7572. [CrossRef]

43. Xu, P.; Phelan, D.; Jeong, J.S.; Mkhoyan, K.A.; Jalan, B. Stoichiometry-driven metal-to-insulator transition in NdTiO$_3$/SrTiO$_3$ heterostructures. *Appl. Phys. Lett.* **2014**, *104*, 082109. [CrossRef]

44. Sitaputra, W.; Sivadas, N.; Skowronski, M.; Xiao, D.; Feenstra, R.M. Oxygen vacancies on SrO-terminated SrTiO$_3$(001) surfaces studied by scanning tunneling spectroscopy. *Phys. Rev. B* **2015**, *91*, 205408. [CrossRef]

45. Yu, P.; Zhang, J. Some interesting properties of black hydrogen-treated TiO$_2$ nanowires and their potential application in solar energy conversion. *Sci. China Chem.* **2015**, *58*, 1810–1815. [CrossRef]

Publisher's Note: MDPI stays neutral with regard to jurisdictional claims in published maps and institutional affiliations.